Fast multicomponent cat-state generation under resonant or strong-dressing Rydberg-Kerr interaction

Mohammadsadegh Khazali [*]
Department of Physics, University of Tehran, Tehran 14395-547, Iran

(Received 9 February 2024; revised 3 May 2024; accepted 6 May 2024; published 20 May 2024)

Cat states are maximally entangled states with applications in metrology and fault-tolerant quantum computation. Experiments have revealed that Rydberg collective avalanche decoherence acts as a bottleneck for cat creation with Rydberg atoms. This process initiates after the blackbody-radiation-induced decay of Rydberg atoms and sets a strong limit on the cat creation time. These findings necessitate the exploration of new ideas to accelerate current Rydberg cat schemes. To enhance the interaction-to-loss ratio, this paper delves into cat-state formation in the strong-Rydberg-dressing regime, uncovering the emergence of cat states despite the presence of complex orders of nonlinearities. This unexplored regime demonstrates the potential for rapid cat-state formation, which is particularly beneficial for operation in typical two-dimensional lattices in Rydberg laboratories. In an extreme case, this paper demonstrates that second-order nonlinearity could be isolated under resonant Rydberg driving if a large number of atoms are accommodated inside the blockade volume. The resonant model significantly enhances the interaction-to-loss ratio while circumventing the adiabaticity condition, allowing fast switching of lasers. In addition, this paper presents a method for generating multicomponent cat states, which are superpositions of m coherent spin states ($|m\text{-CSS}\rangle$). The maximum value of m is determined by the number of atoms within the blockade radius, where $m = \sqrt{N}$. The states with larger m are more robust against the presence of multiple orders of nonlinearity in the strong-dressing Hamiltonian and are accessible in a much shorter time compared to traditional two-component cat states.

DOI: 10.1103/PhysRevA.109.053716

I. INTRODUCTION

The nonlinear interaction resulting from Rydberg dressing has potential applications in various areas, including spin squeezing [1–5], the generation of Schrödinger's cat states [6–9], and the fields of many-body physics and quantum materials [10–16]. Until now, efforts to isolate the quadratic order of nonlinearity have been confined to far-off-resonant laser driving that weakly dresses the excited states with strongly interacting Rydberg states, a condition known as the weak-dressing regime. This quadratic nonlinearity was assumed to be a coherent candidate for making cat states [7,8]. Cat states are highly fragile, as a single decay can result in the complete destruction of entanglement. Experimental endeavors have encountered a significant obstacle in the form of collective avalanche loss [16,17], necessitating any cat proposal to operate within a specific time window to keep the chance of decay induced by blackbody radiation (BBR) below 20% [16]. However, the small interaction-to-loss ratio in the weak-dressing regime does not facilitate the generation of even small cat states, especially in the typical two-dimensional (2D) lattices available in most Rydberg laboratories. To address these challenges, this paper delves into the unexplored strong-dressing regime to enhance the interaction-to-loss ratio. Our findings indicate that approaching resonant Rydberg driving significantly boosts the operation speed.

Deviating from the conventional weak-dressing regime in typical small ensembles ($N \ll 400$), the exploration of stronger-dressing effects amplifies many-body interactions and unlocks higher orders of nonlinearities. In the context of employing two distinct Rydberg-dressing methodologies for cat-state generation [7,8], previous studies have highlighted the susceptibility of the Lipkin-Meshkov-Glick model to mixed nonlinearities [8]. Conversely, our investigation reveals that in the Yurke-Stoller framework [7,18] the impact of higher-order nonlinear terms could be less detrimental. Taking a different approach to this challenge, this paper showcases the isolation of quadratic nonlinearity in an extreme scenario, specifically during resonant Rydberg driving when a substantial number of atoms ($N \gtrsim 400$) are enclosed within the blockade radius. This breakthrough leads to a notable enhancement of the interaction-to-loss ratio, marking a significant stride towards the creation of large entangled states.

While there are multiple measures for quantumness, an intriguing figure of merit could be the number of superposition states that elements could possess simultaneously. Yurke and Stoller [18] discussed the formation of two-component cat states $|2\text{-CSS}\rangle$ under a sole even term of nonlinearity $U \propto N_e^{2k}$. This state is equivalent to the superposition of two coherent spin states pointing in opposite directions on the Bloch sphere. They also highlighted the formation of four-component cats $|4\text{-CSS}\rangle$ under an isolated odd order $U \propto N_e^{2k+1}$. This paper extends that model to create a superposition of m coherent spin states $|m\text{-CSS}\rangle$ with $m \leqslant \sqrt{N}$, where N is

*mskhazali@ut.ac.ir

the number of atoms. Our numerical study reveals that as we move towards a strong-dressing regime, cat states with larger m experience less fidelity reduction and have a much shorter creation time than two-component cat states. The application of the $|m\text{-CSS}\rangle$ state in metrology yields a signal that is periodic in the metrological phase divided by m, reducing the inversion region of the dynamic range of the signal.

Despite the benefits of the strong-dressing regime, the absence of an analytical model describing the interaction profile at this regime [5] has hindered mean-field studies on this unexplored range of parameters. Appendix A investigates an analytic form of the interaction profile involving two- and three-body interactions, providing insights into the effects of lattice geometry and controlling parameters on enhancing specific orders of nonlinearities. Furthermore, it opens new opportunities to study the dynamics of Rydberg-dressed Bose-Einstein condensates [11,12] under a stronger-dressing regime using mean-field theory.

This paper is structured as follows: Sec. II elucidates the traditional concept of Rydberg dressing and explores the relation between dressing strength and the order of nonlinear terms within the Hamiltonian. In Sec. III, the formation of $|m\text{-CSS}\rangle$ states is expounded upon. Furthermore, Sec. IV delves into the benefits derived from transitioning from weak- to strong-dressing techniques. The formulation of the Kerr Hamiltonian for resonant Rydberg driving and its application in cat-state generation are detailed in Sec. V. Last, an analysis of many-body interactions under strong dressing is provided in Appendix A.

II. DRESSING INTERACTION

When all atoms are accommodated within the blockade radius, the dressing laser connects the state without Rydberg excitation $|\psi_0\rangle = \otimes_i|\phi_i\rangle$ (where $\phi \in e, g$) to a state where only one atom in the $|e\rangle$ level is excited to the Rydberg state $|\psi_1\rangle = \sum_i |\phi_1 \cdots r_i \cdots \phi_N\rangle$ with a collective Rabi frequency of $\sqrt{N_e}\Omega_r$ and laser detuning Δ. Here N_e represents the number of atoms in the excited state $|e\rangle$. During the Rydberg-dressing process, the collective light shift experienced by the ground dressed state can be obtained as

$$H_{\text{exact}} = \frac{\Delta}{2}\left(1 - \sqrt{1 + \frac{\hat{N}_e\Omega_r^2}{\Delta^2}}\right). \tag{1}$$

This light shift can be Taylor expanded in the weak-dressing regime ($\frac{N_e\Omega^2}{\Delta^2} \ll 1$) as

$$H_{\text{w}} = -\frac{1}{4}\frac{\hat{N}_e\Omega^2}{\Delta} + \frac{1}{16}\frac{\hat{N}_e^2\Omega^4}{\Delta^3} - \frac{1}{32}\frac{\hat{N}_e^3\Omega^6}{\Delta^5} + \frac{5}{256}\frac{\hat{N}_e^4\Omega^8}{\Delta^7} + O(\hat{N}_e^5). \tag{2}$$

Going to stronger dressing with larger $N_e\frac{\Omega^2}{\Delta^2}$ activates the higher orders of nonlinearity and raises the many-body interaction terms in the Hamiltonian (see Appendix A).

The binary-dressing-interaction profiles are presented by solid lines in Fig. 1(b). They are derived from the steady state of the master equation encountering laser couplings, dipolar Rydberg interaction and spontaneous emission from the

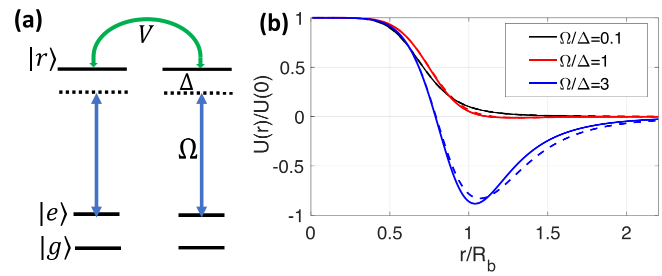

FIG. 1. Transition from weak to strong Rydberg dressing and resonant driving. (a) Level scheme; the spin of atoms consists of $|g\rangle$ and $|e\rangle$ electronic states. The desired Kerr-type interaction is generated by off-resonant laser driving of atoms in the $|e\rangle$ state to the Rydberg level. This paper studies the Kerr-type interaction in the transition from weak $\Omega \ll \Delta$ to the strong-dressing regime $\Omega \gg \Delta$ and introduces the resonant-driving $\Delta = 0$ Kerr Hamiltonian. (b) The binary-dressing-interaction profile derived from the steady state of the master equation. For both weak and strong dressing, the homogeneous soft core is provided for interatomic distances below $R_b/2$. The blockade radii in the weak- and strong-dressing regimes are defined by $R_b = (C_6/\Delta)^{1/6}$ and $R_b = (C_6/\Omega)^{1/6}$, respectively. The interaction is scaled by U_0, which is the exact dressing interaction for totally blockaded atoms.

Rydberg level (see Appendix B). Dressing interaction features a soft core within the blockade radius R_b over which the interaction makes the two Rydberg excitations out of resonance with the laser and forms the effective interaction potentials of Eq. (1). The blockade radius in the weak and strong dressing regimes are defined by $R_b = (C_6/\Delta)^{1/6}$ and $R_b = (C_6/\Omega)^{1/6}$ respectively. In the extreme limit of strong dressing where $\Omega > \Delta$, the interaction would be comparable with the Rabi frequency around R_b and causes blockade leakage. This populates more than one Rydberg atom featuring strong dipolar interaction, represented by an interaction peak in the blue line in Fig. 1(b). At further distances the $1/r^6$ van der Waals tail could be recognized in both weak and strong dressing. The dashed lines in Fig. 1(b) represent the interaction of three atoms on an equilateral triangle with side length r.

III. MAKING SUPERPOSITION OF m-CSS

A coherent spin state (CSS) is defined as a direct product of single-spin states [19],

$$|\theta, \phi\rangle = \otimes_{i=1}^N[\cos\theta|g\rangle_i + \sin\theta e^{i\phi}|e\rangle_i], \tag{3}$$

where all the spins are pointing in the same direction and ϕ and θ are the angles on the (collective) Bloch sphere. The CSS can also be represented as [19]

$$|\eta\rangle = |\theta, \phi\rangle = (1 + |\eta|^2)^{-N/2}\sum_{N_e=0}^{N}\eta^{N_e}\sqrt{C(N, N_e)}|N; N_e\rangle, \tag{4}$$

where $\eta = \tan(\theta/2)e^{-i\phi}$, $C(N, N_e) \equiv \binom{N}{N_e}$, and $|N; N_e\rangle = \frac{1}{\sqrt{C(N,N_e)}}\sum_{i1<i2<\cdots<iN_e}^{N}|g_1 \cdots e_{i1} \cdots e_{iN_e} \cdots g_N\rangle$ is the Dicke state of N_e excited atoms, where $|N; N_e\rangle$ is an alternative representation of the $|J\,M\rangle$ basis with $N = 2J$ and $N_e = J + M$.

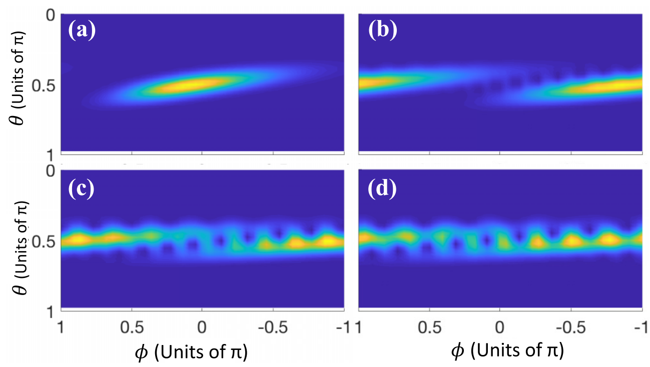

FIG. 2. The physics of multicomponent cat creation: The quadratic interaction term leads to varying rotation speeds around J_z for different $|N_e\rangle$ elements, spanning the range $N_e^{\max} - N_e^{\min} = 2\sqrt{N}$. This causes (a) stretching of the initial CSS over the equator, (b) and (c) constructive and destructive interferences as the squeezed state's head and tail meet and pass through each other, and (d) formation of the first m-CSS superposition after a rotation difference of $\Delta\phi = 4\pi$, allowing for interference to spread all over the equator.

Considering the time evolution of the CSS [Eq. (4)] under the dressing Hamiltonian [Eq. (2)], the linear term in N_e preserves the CSS and generates only a rotation around J_z, while the quadratic term χN_e^2 causes spin-squeezing over the Bloch sphere, see Fig. 2. After the CSS is squeezed over the equator, it starts to form a superposition of m-CSSs at $t_m = \frac{2\pi}{m\chi}$:

$$|m\text{-CSS}\rangle = \frac{1}{\sqrt{m}} \sum_{k=1}^{m} e^{i\alpha_k} \left|\theta = \pi/2; \phi = k\frac{2\pi}{m} + \phi_0\right\rangle. \quad (5)$$

The values of α_k are obtained numerically in Appendix D. Continuing the interaction, the revival of the initial CSS can be observed at t_1. This revival can be used as proof of the successful creation of a quantum superposition at t_m since a statistical mixture of CSSs at t_m would evolve into another mixture of separate peaks (see Appendix C and Fig. 6).

For the weak dressing, where the third order of nonlinearity is negligible, the operation time $t_m = 2\pi/m\chi$ will perfectly match the numerical simulation used in Fig. 3. Going to strong dressing, the operation time will be longer than t_m. This is because the third order of nonlinearity has the opposite sign of the second order [see Eq. (2)], which makes the process a bit slower. However, the trend remains positive in terms of enhancing coherence.

Here we discuss the physics that determines the maximum number m of CSSs that could be formed in a superposition state. The population difference of N_e in the initial CSS is given by $N_e^{\max} - N_e^{\min} = 2\sqrt{N}$. Hence, the quadratic term of interaction will cause different rotation speeds around J_z for different $|N_e\rangle$ elements of the initial CSS in Eq. (4). This will stretch the initial CSS over the equator. After the head and tail of the squeezed state meet and go through each other, they form constructive and destructive interferences, which is shown as the superposition of CSSs (see Fig. 2). Hence, the minimum required time to form the superposition is defined by the time that the head and tail of the squeezed state are stretched over $\Delta\phi = 4\pi$ to spread the interference all over the Bloch sphere equator. Considering the difference in rotation speed under the quadratic term, the minimum dressing time that is required for the superpositions to appear will be $t_{\min} = \frac{4\pi}{(N_e^{\max} - N_e^{\min})\Omega^4/16\Delta^3} = \frac{4\pi}{2\sqrt{N}\chi}$. The $|m\text{-CSS}\rangle$ will be formed only if its operation time $t_m = 2\pi/m\chi$ occurs after the spread of interference all over the equator at $t_{\min}$ (see Fig. 2). Hence, the maximum number of m-CSS superpositions that can be formed will be determined by the number of spins in the operation $m = \sqrt{N}$. One should note that this argument is derived in the weak-dressing regime and going to strong dressing changes the operation times.

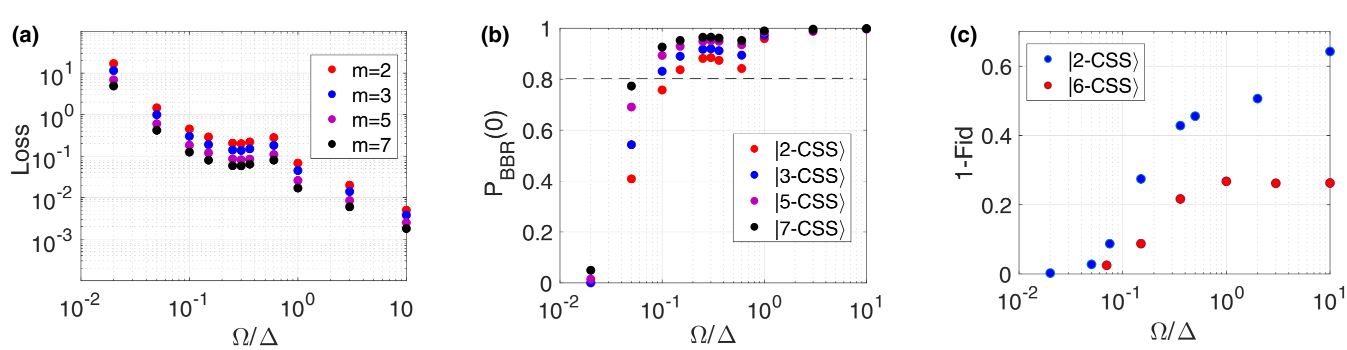

FIG. 3. Transition from weak to strong dressing. (a) The population loss over the $|m\text{-CSS}\rangle$ generation $P_r\Gamma_r t_m$ is plotted as a function of dressing strength. Here constant detuning $\Delta/2\pi = 0.02$ GHz in addressing the $|53P_{3/2}, 3/2\rangle$ state and $N = 48$ atoms are considered. At very weak dressing with quadratic nonlinearity, the interaction-to-loss ratio scales by $\Omega^2/4\Delta$, and hence, the loss drops by Ω^{-2}. In the intermediate regime, the counterrotation corresponding to the third order of nonlinearity slows the process down and hence reduces the loss-rate reduction. Later, the Rydberg population in the blockade radius reaches the maximum limit of 1 while the interaction keeps enhancing $\propto\Omega$ in the strong-dressing regime, leading to loss suppression scaling by Ω^{-1}. (b) The Poissonian probability of not having any BBR-induced depopulation $P_{\mathrm{BBR}}(0)$ is plotted as a function of dressing strength. Going to resonance is important, especially for large-N cat states, to ensure the operation time finishes before the collective avalanche loss starts. (c) The outcome infidelity as a function of dressing strength. States with larger m are less sensitive to the effects of higher-order nonlinearities. The cryogenic environment with $T = 77$ K is considered in the calculations in (a) and (b).

IV. ADVANTAGE OF STRONG DRESSING

Cat states are extremely fragile with respect to decoherence, where a single decay leads to total destruction of entanglement. The decoherence is the bottleneck that limits cat states to tens of atoms in atomic systems. For constant ensemble size N, going to strong dressing with larger Ω/Δ is favorable for enhancing the interaction-to-loss ratio. To make a simple argument, let us consider the weak-dressing regime, where the dominant term of interaction in the soft core is $\chi N_e^2 = N_e^2\Omega^4/16\Delta^3$, while the loss rate from the Rydberg population $P_r = N_e(\frac{\Omega}{2\Delta})^2$ is given by $P_r\gamma_r$, with γ_r being the loss rate from the Rydberg levels [20]. Considering the symmetry of states around the Bloch sphere's equator, N_e can be replaced by $N/2$ in this scaling argument. Hence, the interaction-to-loss ratio scales by $\frac{N\Omega^2}{4\Gamma\Delta}$. When transitioning to strong dressing, it becomes necessary to incorporate higher orders of expansion in Eq. (2). While the inclusion of odd terms may cause a deviation in the scaling from the specified interaction-to-loss ratio, the overall trend still favors moving towards strong dressing, as demonstrated below.

Figure 3(a) plots the Rydberg depopulation over the $|m\text{-CSS}\rangle$ generation as a function of dressing strength. For simplicity both the spontaneous emission and BBR-induced depopulation are considered as loss terms, which adds up to a 4.8-ms^{-1} decoherence rate for $|53P_{3/2}, 3/2\rangle$. Considering a 2D lattice with lattice constant $a = 532$ nm [21], the laser detuning of $\Delta/2\pi = 20$ MHz accommodates $N = 48$ atoms well within the soft-core area $R_b/2$. At very weak dressing with quadratic nonlinearity the interaction-to-loss ratio scales by $\Omega^2/4\Delta$, and hence, the loss drops by Ω^{-2}. In the intermediate regime the counterrotation effects of the third order of nonlinearity suppress the interaction and hence slow down the rate of loss reduction. At stronger dressing, the Rydberg population in the blockade radius reaches the maximum limit of 1, after which the loss rate remains constant. This happens while the interaction continues to get enhanced $\propto\Omega$ in the strong-dressing regime [see Eq. (8)], leading to loss suppression that is scaled by Ω^{-1}.

Other than the spontaneous emission and BBR-induced depopulation of Rydberg states discussed above, experiments [16,17] have observed a collective decoherence that is triggered by the BBR-induced depopulation of the Rydberg atoms. The BBR-induced depopulation to neighboring $n'P$ Rydberg states invokes a strong resonant dipolar interaction with the targeted nS state, resulting in an anomalous line broadening. This further enhances the depopulation rate, leading to a collective avalanche decoherence. Figure 3(b) plots the Poissonian probability of not losing any Rydberg atoms due to the BBR-induced depopulation $P_{\text{BBR}}(0) = \exp(-P_r\Gamma_{\text{BBR}}t_m)$, where the value of Γ_{BBR} can be found in [20]. Reference [16] observed that the avalanche decoherence starts only when $P_{\text{BBR}}(0)$ drops below 82%. Figure 3(b) shows the reduction of $P_{\text{BBR}}(0)$ while going towards the strong dressing. Going towards resonance would be vital for operations with large numbers of atoms in dense three-dimensional lattices.

While the transition to a strong-dressing regime is crucial for preventing decay over large-scale cat creation time, the mixed nonlinear terms lead to deviations from the targeted state. Figure 3(c) compares the system state $|\psi(t)\rangle$ evolving under the exact Hamiltonian from Eq. (1) with the targeted state $|m\text{-CSS}\rangle$ defined in Eq. (5). The fidelity is determined by optimizing the operation time and the parameters of the targeted state using

$$F = \max_{\alpha_k,\phi_0,t} \left| \langle\psi(t)| \frac{1}{\sqrt{m}} \sum_{k=1}^{m} e^{i\alpha_k} \middle| \theta = \pi/2; \phi = \frac{2\pi k}{m} + \phi_0 \right\rangle \right|^2. \tag{6}$$

Figure 3(c) exclusively considers the effects of mixed nonlinear terms without accounting for decoherence. The states with larger m components are more robust against the presence of mixed nonlinearities. This is quantified for the cases of $|2\text{-CSS}\rangle$ and $|6\text{-CSS}\rangle$ in Fig. 3(c) but could not be calculated for larger m due to the large dimension of optimization. However, the Q function of $|33\text{-CSS}\rangle$ with $N = 1000$ atoms generated under resonant driving in Fig. 4 shows a high-fidelity outcome. Some examples of the Husimi Q function in the weak- and strong-dressing regimes are plotted in Fig. 6 in Appendix D.

While transitioning to a stronger dressing changes the outcome from the desired states, the sharp diving of the operation time and dissipation that allows the generation of a cat state in the first place outweigh the deviation from an exact $|m\text{-CSS}\rangle$ with large m. Consequently, depending on the application,

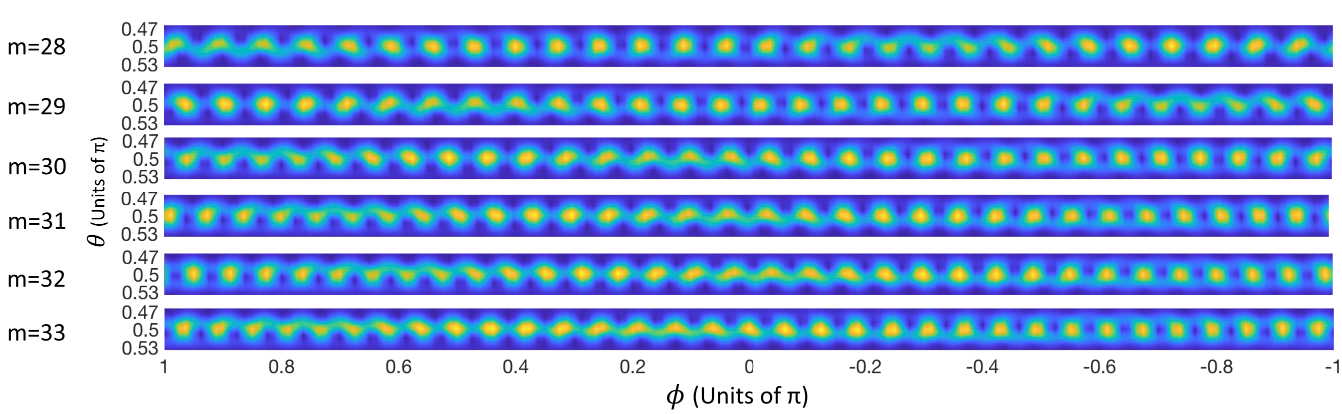

FIG. 4. Cat formation under the resonant-Rydberg-driving Hamiltonian in Eq. (7) applied on $N = 1000$ atoms.

enhancing the coherence or size of the entangled state may justify the reduction in fidelity.

V. GOING TO RESONANCE

Resonant-Rydberg-driving Kerr Hamiltonian. As explained above, approaching the resonance regime for the Rydberg exciting laser improves the interaction-to-loss ratio. This section discusses the cat generation under the resonant Rydberg excitation. Accommodating all the atoms inside the blockade radius, the effective interaction is given by

$$H_{\rm res} = \sqrt{\hat{N}_e}\Omega, \tag{7}$$

where N_e is the number of atoms in $|e\rangle$ state. Having a large number of atoms and initializing the CSS on the equator of the Bloch sphere, the average number of excited atoms $\bar{N}_e = N/2$ is much larger than the deviation $\hat{N}_e - \bar{N}_e$, which is given by the radius of CSS, i.e., $\sqrt{N}$. Hence, in the regime of a large number of atoms $N/2 \gg \sqrt{N}$, the resonance Hamiltonian of Eq. (7) can be expanded:

$$\begin{aligned}\hat{H}_{\rm res} &= \Omega\sqrt{\bar{N}_e}\left(1+\frac{\hat{N}_e-\bar{N}_e}{\bar{N}_e}\right)^{1/2} = \Omega\sqrt{\bar{N}_e}\left(1+\frac{\hat{N}_e-\bar{N}_e}{2\bar{N}_e}-\frac{(\hat{N}_e-\bar{N}_e)^2}{8\bar{N}_e^2}+\frac{(\hat{N}_e-\bar{N}_e)^3}{16\bar{N}_e^3}-\cdots\right)\\ &\approx \Omega\sqrt{\bar{N}_e}\left[\frac{5}{16}+\frac{15}{16}\frac{\hat{N}_e}{\bar{N}_e}-\frac{5}{16}\left(\frac{\hat{N}_e}{\bar{N}_e}\right)^2+\frac{1}{16}\left(\frac{\hat{N}_e}{\bar{N}_e}\right)^3-\cdots\right] \approx \Omega\left[\frac{5}{16}\sqrt{\frac{N}{2}}+\frac{15}{16}\sqrt{\frac{2}{N}}\hat{N}_e-\frac{5}{16}\sqrt{\frac{2^3}{N^3}}\hat{N}_e^2+\frac{1}{16}\sqrt{\frac{2^5}{N^5}}\hat{N}_e^3\right].\end{aligned} \tag{8}$$

As an example, the formation of a few $|m\text{-CSS}\rangle$ with $N = 1000$ atoms under the resonant-driving Hamiltonian in Eq. (7) are plotted in Fig. 4. The cat creation times obtained from the numerics are $\chi_2^{\rm res} \times [t_{33}, t_{27}, t_{21}, t_{14}, t_7, t_4, t_3, t_2] = [0.236, 0.289, 0.373, 0.563, 1.132, 2, 2.655, 4.061]$, which are normalized by the dominant order of nonlinearity $\chi_2^{\rm res} = \frac{5}{16}\sqrt{(\frac{2}{N})^3}\Omega$. The $|33\text{-CSS}\rangle$ state is formed 17 times faster than the conventional $|2\text{-CSS}\rangle$ cat state.

Given that the ensemble is located within the blockade radius, the Rydberg population is fixed at 1 in the resonant-driving model. Consequently, the loss can be calculated as the product of the operation time and the Rydberg loss rate. For instance, let us consider the resonant driving of $N = 1000$ ^{87}Rb atoms to the $|80S_{1/2}\rangle$ state with a Rabi frequency of $\Omega/2\pi = 70$ MHz. In the cryogenic environment at $T = 77$ K, the Rydberg decay rate is $\Gamma_r = 2400\ \text{s}^{-1}$. Numerically, the operation times for creating the $|33\text{-CSS}\rangle$ and $|2\text{-CSS}\rangle$ states are found to be $t_{33} = 0.236/\chi_2^{\rm res}$ and $t_2 = 4/\chi_2^{\rm res}$, respectively. The corresponding Poissonian probabilities of not losing any atoms over operation times t_{33} and t_2 are 98% and 66%, respectively. In a scaling argument, as the principal quantum number increases, the Rydberg decay rate is suppressed as $\Gamma_r \propto n^{-3}$, while the interaction is enhanced as $C_6 \propto n^{11}$, allowing for stronger laser driving and faster operation for a constant blockade radius. Consequently, the atom loss over cat creation scales inversely with the principal number as n^{-14} for a constant atom number N.

A note on adiabaticity. Considering the off-resonant Rydberg dressing as explained in Sec. II, the laser couples two states $|\psi_0\rangle$ and $|\psi_1\rangle$ with collective Rabi frequency $\sqrt{N_e}\Omega_r$ and detuning Δ. The time evolution of dressed eigenstates $|\tilde{\psi}_\pm\rangle$ is given by

$$i\frac{\partial}{\partial t}\begin{pmatrix}|\tilde{\psi}_-\rangle\\ |\tilde{\psi}_+\rangle\end{pmatrix} = \begin{pmatrix}\mathcal{E}_- & -i\dot{\theta}/2\\ i\dot{\theta}/2 & \mathcal{E}_+\end{pmatrix}\begin{pmatrix}|\tilde{\psi}_-\rangle\\ |\tilde{\psi}_+\rangle\end{pmatrix}, \tag{9}$$

where $\mathcal{E}_\pm = \frac{\Delta}{2}(1 \pm \sqrt{1+\frac{N_e\Omega^2}{\Delta^2}})$ are the energies of ground and excited dressed states and $\dot{\theta} = \frac{\sqrt{N_e}\Omega\dot{\Delta}-\sqrt{N_e}\Delta\dot{\Omega}}{N_e\Omega^2+\Delta^2}$. In the case of nonzero detuning, it is important to keep the off-diagonal terms small to minimize the population scattering to the other eigenstate, which is quantified by $\dot{\theta}^2/E_+^2$. The scattered population will remain in the Rydberg state after switching of the laser, which results in the distortion of cat states. On the other hand, the off-diagonal terms will not appear when the laser becomes in resonance with the Rydberg level. This will bring the advantage of fast switching of the laser in resonant driving.

VI. CONCLUSION

In the thriving field of Rydberg technology [22–30], Rydberg dressing plays an important role in the implementation of quantum matters and making large-scale entanglement. This paper delves into the generation of multicomponent cat states through both strong Rydberg dressing and resonant Rydberg driving, departing from previous research that primarily focused on the weak-dressing regime to isolate the second order of nonlinearity. By approaching resonance, the interaction-to-loss ratio is enhanced, enabling successful operation termination before the onset of BBR-induced collective avalanche decoherences. The findings here demonstrate that resonant Rydberg driving can effectively isolate quadratic nonlinearity with a large number of atoms accommodated within the blockade volume.

Moreover, this paper introduced a method to create multicomponent cat states on significantly shorter timescales compared to traditional two-component cat states. These states exhibit reduced sensitivity to mixed nonlinearity orders, making them an attractive option for generating large-scale entangled states crucial for applications in metrology and quantum error correction. Last, Appendix A presents a perturbative analytic formula for strong-dressing interactions, suggesting the optimization of lattice geometry to resonate and enhance specific orders of nonlinearity.

ACKNOWLEDGMENT

The author acknowledges motivating discussions with N. Schine.

APPENDIX A: MANY-BODY INTERACTION AT STRONG DRESSING

To investigate the strong-dressing regime in mean-field formalism, one needs an analytic formula for the interaction profile. The profile of weak-dressing interaction has been formulated in a perturbative approach that covers up to the two-body interaction [12]. Going to stronger dressing, the effects of higher-order terms would be magnified. This Appendix looks into the analytical profile of the interaction up to the third order of nonlinearity.

Considering N atoms in an optical lattice, for each pair of atoms excited to the Rydberg level $|r\rangle$ and separated by $\mathbf{x}_{ij} = \mathbf{x}_i - \mathbf{x}_j$, where $\mathbf{x}_i$ is the position of the ith atom, the binary interaction is $V_{ij} = C_6/x_{ij}^6$. Here the quantization axis is considered to be perpendicular to the lattice plane to preserve the isotropy of interaction. The dressing potential $U(\mathbf{x}_1 \cdots \mathbf{x}_{N_e})$ of the state $|\psi(\mathbf{x}_1 \cdots \mathbf{x}_{N_e})\rangle$, with N_e atoms in $|e\rangle$ being dressed with Rydberg level $|r\rangle$, is calculated under the condition of $(\frac{\Omega}{2\Delta})^2 \ll 1$ by applying perturbation theory:

$$\frac{U}{\Delta}|\psi\rangle = \left(\sum_{i=1}^{N}\hat{\sigma}_{rr}^{i} + \frac{1}{\Delta}\sum_{i<j}V_{ij}\hat{\sigma}_{rr}^{i}\hat{\sigma}_{rr}^{j}\right) + \frac{\Omega}{2\Delta}\sum_{i=1}^{N}\left(\hat{\sigma}_{re}^{i} + \hat{\sigma}_{er}^{i}\right)|G\rangle, \tag{A1}$$

where the first and second parentheses separate the unperturbed and perturbed parts of Hamiltonians.

The contributions from the second- and fourth-order perturbations are calculated as [12]

$$U^{(2)} = -\frac{\Omega^2}{4\Delta}N,$$
$$U^{(4)} = \frac{\Omega^4}{16\Delta^3}\sum_{i<j}\left[\frac{1}{\left(1+\frac{V_{ij}}{2\Delta}\right)} - 1\right], \tag{A2}$$

where the former is the sum of the single-atom light shift and the latter encounters the two-body interactions among atoms. In the limit of strong interaction ($V \to \infty$) these terms reproduce the first two terms of collective light-shift expansion in Eq. (2).

Going to a stronger dressing regime with a non-negligible third order of nonlinearity $(N_e\frac{\Omega^2}{4\Delta^2})^3$, the sixth-order perturbation must be taken into account. Here different configurations of the six photon transitions in the perturbative ladder are plotted in Fig. 5, which includes the two-body and three-body interactions. The sixth correction of the interaction profile is given by

$$\begin{aligned} U^{(6)} = \frac{\Omega^6}{2^6\Delta^5}\Bigg\{ & -2N^3 + \left[\sum_{k=1}^{N}(1)\right]\sum_{i\neq j}\frac{4}{2 - V_{ij}/\Delta} \\ & + \sum_{i\neq j}\frac{2}{2-V_{ij}/\Delta}\left(\sum_{k\neq i}\frac{2}{2-V_{ik}/\Delta} + \sum_{k\neq j}\frac{2}{2-V_{jk}/\Delta}\right)\times 2 \\ & - \sum_{i\neq j}\frac{2}{2-V_{ij}/\Delta}\left(\sum_{i}\frac{1}{2-V_{ij}/\Delta} + \sum_{j}\frac{1}{2-V_{ij}/\Delta}\right) \\ & - \sum_{(ijk)\neq}\left(\frac{2}{2-V_{ij}/\Delta} + \frac{2}{2-V_{ik}/\Delta} + \frac{2}{2-V_{jk}/\Delta}\right)^2 \\ & \times \frac{1}{3 - V_{ij}/\Delta - V_{ik}/\Delta - V_{jk}/\Delta}\Bigg\}. \end{aligned} \tag{A3}$$

Comparing the terms in Eqs. (A2) and (A3), one can see that the ratio of Δ/V in a lattice with a given geometry could be used as a knob to control the relative strengths of different nonlinear terms. For example, expanding this trend to higher orders, one can see that in a square (triangle) lattice, the fourth (sixth) order of nonlinearity will get enhanced around $\Omega = \Delta$. This could be instrumental in isolating the fourth order of nonlinearity with potential applications in cat-state error-correction codes [31].

APPENDIX B: NUMERICAL CALCULATION OF THE INTERACTION PROFILE

The level scheme depicted in Fig. 1(a) pertains to three-level rubidium atoms undergoing off-resonant excitation to the highly excited Rydberg state $|r\rangle$. The laser-driving Hamiltonian for the ith atom is given by $H_i = \frac{\Omega}{2}(\hat{\sigma}_{re}^{i} + \hat{\sigma}_{er}^{i}) - \Delta\hat{\sigma}_{rr}^{i}$, where $\sigma_{\alpha,\beta} = |\alpha\rangle\langle\beta|$ and Ω and Δ represent the Rabi frequency and detuning of the transition, respectively. The van der Waals interaction between Rydberg atoms, denoted as $V_{ij} = C_6/r_{ij}^6\sigma_{rr}^{i}\sigma_{rr}^{j}$, is a function of the interatomic distance r_{ij}. The total multiatom dressing Hamiltonian is expressed as $H_d = \sum_i \hat{H}_i + \sum_{i<j} V_{ij}$. The dynamics of the system under the Rydberg-dressing interaction is governed by the master equation, which can be represented as

$$\partial_t\hat{\rho} = -i[H_d, \hat{\rho}] + \sum_i \mathcal{L}_i(\hat{\rho}), \tag{B1}$$

where the Liouvillian operator $\mathcal{L}_i(\rho) = c\rho_i c^\dagger - 1/2(c^\dagger c\rho_i + \rho_i c^\dagger c)$ in Lindblad form describes the single-particle dissipation affecting the internal state dynamics, with $c = \sqrt{\gamma_r}|e\rangle\langle r|$ governing the spontaneous emission from the Rydberg state.

Upon considering the steady state ρ from Eq. (B1), the interaction can be calculated as

$$U = \mathrm{Tr}[\rho H_d]. \tag{B2}$$

Figure 1(b) illustrates the dressing interaction profile for two atoms separated by r (solid lines) and three atoms arranged in an equilateral triangle with sides of length r (dashed lines) for various dressing strengths. To present the effective interaction, the background interaction-independent light shift $U(r = \infty)$, which generates only a constant phase, is subtracted. The blockade radius is defined as $R_b = (C_6/\Delta)^{1/6}$ in the weak-dressing regime and as $R_b = (C_6/\Omega)^{1/6}$ in the strong-dressing regime. It is evident from Fig. 1(b) that in both weak and strong dressings, as long as the atoms are within the soft core

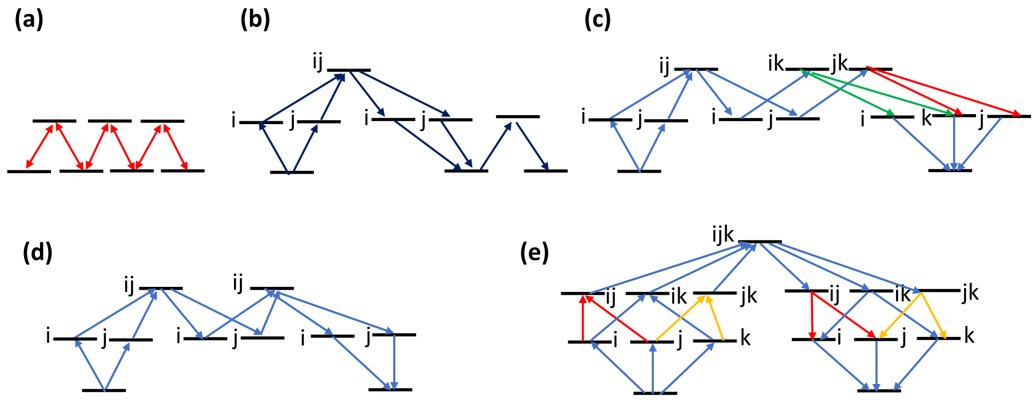

FIG. 5. Perturbation paths used to calculate $U^{(6)}$ in Eq. (A3). Indices i, j, and k label different atoms excited to the Rydberg state.

with a radius of $R_b/2$, the interaction becomes independent of atomic distance and is defined by solely the collective light shift, characterized by the number of atoms and laser-driving parameters.

APPENDIX C: ASSESSING COHERENCE THROUGH EVOLUTION ANALYSIS

While the Wigner representation effectively visualizes the coherence of superposition in photonic systems through the presence of fringes in phase space, this method cannot be directly applied to coherent spin states (CSSs) in atoms. Instead, the Husimi Q function offers a convenient means of visualizing quantum states by projecting them onto the coherent spin states $|\theta,\phi\rangle$, where the parameters span the Bloch sphere. However, it is important to note that the Husimi Q function alone does not inherently distinguish a cat state, representing a coherent superposition state, from a mixed state. To assess coherence, one can examine the retrieval of a single CSS under the dressing interaction at t_1, as discussed below.

Let us analyze the evolution of the CSS under the second-order nonlinearity $\chi\hat{N}_e^2$. As previously described, the initial CSS $|\eta\rangle$ evolves into $(e^{-i\pi/4}|\eta\rangle + e^{i\pi/4}|-\eta\rangle)/\sqrt{2}$ after duration of dressing t_2 (recall $t_m = \frac{2\pi}{m\chi}$). Following the evolution of the density matrix in the $|\eta\rangle$, $|-\eta\rangle$ basis, the initial state $\rho(0) = \begin{pmatrix}1&0\\0&0\end{pmatrix}$ evolves into $\rho(t_2) = 1/2\begin{pmatrix}1&i\\-i&1\end{pmatrix}$. Subsequently, the same map transfers the state to $\rho(t_1) = \begin{pmatrix}0&0\\0&1\end{pmatrix}$ after another dressing time line t_2 (note $t_1 = 2t_2$). Conversely, if the state at t_2 were a mixed state $\rho_{\rm mixed}(t_2) = 1/2\begin{pmatrix}1&0\\0&1\end{pmatrix}$, it would evolve into another statistical mixture of CSSs $\rho_{\rm mixed}(t_1) = 1/2\begin{pmatrix}1&0\\0&1\end{pmatrix}$ after the same duration of dressing time.

In conclusion, while the Husimi Q function of the cat state $\rho(t_2)$ and a mixed state $\rho_{\rm mixed}(t_2)$ may not be distinguishable, the revival of a CSS at t_1 provides a clear signature of coherence at the earlier time (see Fig. 6). The coherent cat state will evolve into a single CSS, whereas a statistical mixture of CSSs at t_2 will evolve into another mixture of separate peaks at t_1.

APPENDIX D: DEPICTION OF CAT STATES' Q FUNCTION IN WEAK AND STRONG DRESSINGS

Some examples of the Husimi Q function of simulated cat states under the exact Hamiltonian in Eq. (1) in the weak- and strong-dressing regimes are plotted in Fig. 6. Here a 2D lattice with lattice constant $a = 532$nm [21] is considered. Dressing atoms with the $|53P_{3/2}, 3/2\rangle$ Rydberg state with laser detuning of $\Delta/2\pi = 0.02$ GHz accommodates $N = 48$ atoms well within the soft-core region with radius $R_b/2$. In Fig. 6, the first column corresponds to cases where the second order of nonlinearity χ_2 is isolated; in the second column partial involvement of the third order $\chi_3/\chi_2 = 0.06$ is considered, and in the third column, the extreme case in which all orders of nonlinearity are involved in ascending order is applied. The cat-formation process can be observed in the case in which all orders of nonlinearity exist, but with reduced fidelity.

The applied $|m\text{-CSS}\rangle$ that are used to define the fidelity in Figs. 3 and 6 are as follows:

$$|2\text{-CSS}\rangle = [e^{-i\pi/4}|\eta\rangle + e^{i\pi/4}|e^{i\pi}\eta\rangle]/\sqrt{2},$$

$$|3\text{-CSS}\rangle = [e^{-i\pi/3}|\eta\rangle + e^{-i5\pi/3}|e^{i2\pi/3}\eta\rangle + e^{-i5\pi/3}|e^{i4\pi/3}\eta\rangle]/\sqrt{3},$$

$$|3\text{-CSS}\rangle = [e^{-i2\pi/3}|\eta\rangle + e^{-i\pi/3}|e^{i2\pi/3}\eta\rangle + e^{-i\pi/3}|e^{i4\pi/3}\eta\rangle]/\sqrt{3},$$

$$|3\text{-CSS}\rangle = [e^{i2\pi/3}|\eta\rangle + e^{-i2\pi/3}|e^{i2\pi/3}\eta\rangle + e^{-i2\pi/3}|e^{i4\pi/3}\eta\rangle]/\sqrt{3},$$

$$|3\text{-CSS}\rangle = [e^{i\pi/3}|\eta\rangle + e^{-i\pi}|e^{i2\pi/3}\eta\rangle + e^{-i\pi}|e^{i4\pi/3}\eta\rangle]/\sqrt{3},$$

$$|4\text{-CSS}\rangle = [e^{-i\pi/4}|\eta\rangle + |e^{i2\pi/4}\eta\rangle + e^{-i\pi/4}|e^{i4\pi/4}\eta\rangle + e^{-i\pi}|e^{i6\pi/4}\eta\rangle]/\sqrt{4},$$

$$|5\text{-CSS}\rangle = [e^{-i4\pi/5}|\eta\rangle + e^{-i8\pi/5}|e^{i2\pi/5}\eta\rangle + e^{-i4\pi/5}|e^{i4\pi/5}\eta\rangle + e^{-i2\pi/5}|e^{i6\pi/5}\eta\rangle + e^{-i2\pi/5}|e^{i8\pi/5}\eta\rangle]/\sqrt{5},$$

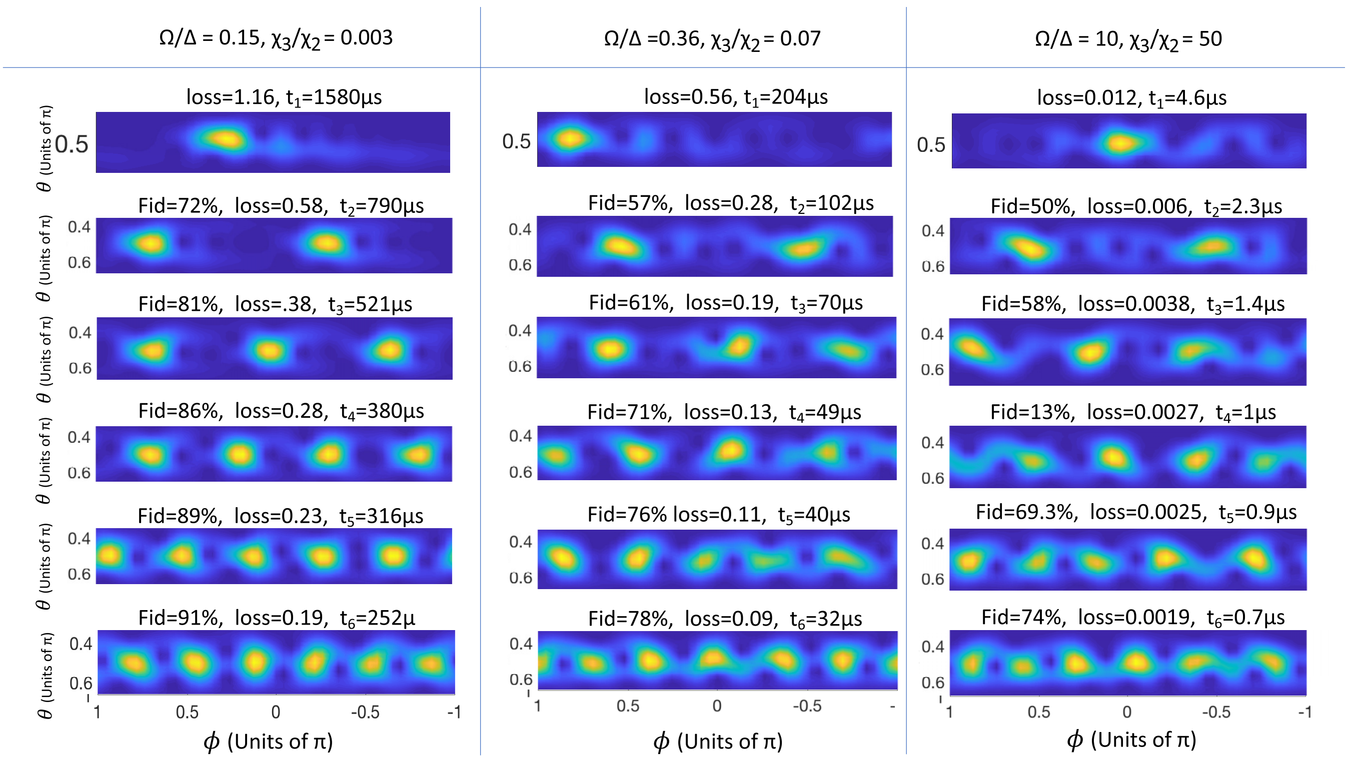

FIG. 6. Transition from a weak- to strong-dressing regime. The revival of a single CSS at time t_1 indicates the coherent superposition of $|m\text{-CSS}\rangle$ states in both the weak- and strong-dressing regimes. The last column contains an ascending contribution of all nonlinear terms in Eq. (2).

$$|5\text{-CSS}\rangle = [e^{-i8\pi/5}|\eta\rangle + e^{-i2\pi/5}|e^{i2\pi/5}\eta\rangle + e^{-i8\pi/5}|e^{i4\pi/5}\eta\rangle + e^{-i6\pi/5}|e^{i6\pi/5}\eta\rangle + e^{-i6\pi/5}|e^{i8\pi/5}\eta\rangle]/\sqrt{5},$$

$$|6\text{-CSS}\rangle = [|\eta\rangle + e^{-i11\pi/6}|e^{i2\pi/6}\eta\rangle + |e^{i4\pi/6}\eta\rangle + e^{-i3\pi/6}|e^{i6\pi/6}\eta\rangle + e^{-i8\pi/6}|e^{i8\pi/6}\eta\rangle + e^{-i3\pi/6}|e^{i10\pi/6}\eta\rangle]/\sqrt{6}.$$

[1] W. J. Eckner, N. D. Oppong, A. Cao, A. W. Young, W. R. Milner, J. M. Robinson, J. Ye, and A. M. Kaufman, Realizing spin squeezing with Rydberg interactions in an optical clock, Nature (London) **621**, 734 (2023).

[2] J. A. Hines, S. V. Rajagopal, G. L. Moreau, M. D. Wahrman, N. A. Lewis, O. Markovic, and M. Schleier-Smith, Spin squeezing by Rydberg dressing in an array of atomic ensembles, Phys. Rev. Lett. **131**, 063401 (2023).

[3] L. I. R. Gil, R. Mukherjee, E. M. Bridge, M. P. A. Jones, and T. Pohl, Spin squeezing in a Rydberg lattice clock, Phys. Rev. Lett. **112**, 103601 (2014).

[4] J. T. Young, S. R. Muleady, M. A. Perlin, A. M. Kaufman, and A. M. Rey, Enhancing spin squeezing using soft-core interactions, Phys. Rev. Res. **5**, L012033 (2023).

[5] J. Van Damme, X. Zheng, M. Saffman, M. G. Vavilov, and S. Kolkowitz, Impacts of random filling on spin squeezing via Rydberg dressing in optical clocks, Phys. Rev. A **103**, 023106 (2021).

[6] A. Omran, H. Levine, A. Keesling, G. Semeghini, T. T. Wang, S. Ebadi, H. Bernien, A. S. Zibrov, H. Pichler, S. Choi, J. Cui, M. Rossignolo, P. Rembold, S. Montangero, T. Calarco, M. Endres, M. Greiner, V. Vuletic, and M. D. Lukin, Generation and manipulation of Schrödinger cat states in Rydberg atom arrays, Science **365**, 570 (2019).

[7] M. Khazali, H. W. Lau, A. Humeniuk, and C. Simon, Large energy superpositions via Rydberg dressing, Phys. Rev. A **94**, 023408 (2016).

[8] M. Khazali, Progress towards macroscopic spin and mechanical superposition via Rydberg interaction, Phys. Rev. A **98**, 043836 (2018).

[9] Y. Y. Jau, A. M. Hankin, T. Keating, I. H. Deutsch, and G. W. Biedermann, Entangling atomic spins with a Rydberg-dressed spin-flip blockade, Nat. Phys. **12**, 71 (2016).

[10] J. Honer, H. Weimer, T. Pfau, and H. P. Büchler, Collective many-body interaction in Rydberg dressed atoms, Phys. Rev. Lett. **105**, 160404 (2010).

[11] M. Khazali, Rydberg noisy dressing and applications in making soliton-molecules and droplet quasicrystals, Phys. Rev. Res. **3**, L032033 (2021).

[12] N. Henkel, R. Nath, and T. Pohl, Three-dimensional roton excitations and supersolid formation in Rydberg-excited Bose-Einstein condensates, Phys. Rev. Lett. **104**, 195302 (2010).

[13] S. Möbius, M. Genkin, A. Eisfeld, S. Wüster, and J. M. Rost, Entangling distant atom clouds through Rydberg dressing, Phys. Rev. A **87**, 051602(R) (2013).

[14] R. Mukherjee, C. Ates, W. Li, and S. Wüster, Phase-imprinting of Bose-Einstein condensates with Rydberg impurities, Phys. Rev. Lett. **115**, 040401 (2015).

[15] A. Pendse, S. Shirol, S. Tiwari, and S. Wüster, Generation and decoherence of soliton spatial superposition states, Phys. Rev. A **102**, 053322 (2020).

[16] J. Zeiher, R. van Bijnen, P. Schauß, S. Hild, J. Choi, T. Pohl, I. Bloch, and C. Gross, Many-body interferometry of a Rydberg-dressed spin lattice, Nat. Phys. **12**, 1095 (2016).

[17] E. A. Goldschmidt, T. Boulier, R. C. Brown, S. B. Koller, J. T. Young, A. V. Gorshkov, S. L. Rolston, and J. V. Porto, Anomalous broadening in driven dissipative Rydberg systems, Phys. Rev. Lett. **116**, 113001 (2016).

[18] B. Yurke and D. Stoler, Generating quantum mechanical superpositions of macroscopically distinguishable states via amplitude dispersion, Phys. Rev. Lett. **57**, 13 (1986).

[19] J. Ma, X. Wang, C. P. Sun, and F. Nori, Quantum spin squeezing, Phys. Rep. **509**, 89 (2011).

[20] I. I. Beterov, I. I. Ryabtsev, D. B. Tretyakov, and V. M. Entin, Quasiclassical calculations of blackbody-radiation-induced depopulation rates and effective lifetimes of Rydberg nS, nP, and nD alkali-metal atoms with $n \leqslant 80$, Phys. Rev. A **79**, 052504 (2009).

[21] C. Weitenberg *et al.*, Single-spin addressing in an atomic Mott insulator, Nature (London) **471**, 319 (2011).

[22] M. Morgado and S. Whitlock, Quantum simulation and computing with Rydberg-interacting qubits, AVS Quantum Sci. **3**, 023501 (2021).

[23] M. Khazali and K. Mølmer, Fast multiqubit gates by adiabatic evolution in interacting excited-state manifolds of Rydberg atoms and superconducting circuits, Phys. Rev. X **10**, 021054 (2020).

[24] M. Khazali, Discrete-time quantum-walk and Floquet topological insulators via distance-selective Rydberg-interaction, Quantum **6**, 664 (2022).

[25] M. Khazali, Quantum information and computation with Rydberg atoms, Iran. J. Appl. Phys. **10**, 19 (2021); Applications of atomic ensembles for photonic quantum information processing and fundamental tests of quantum physics, Ph.D. thesis, University of Calgary, 2016, https://www.proquest.com/openview/b35882136d01bc6643040d8c66c410e6/1?pqorigsite=gscholar&cbl=18750.

[26] M. Khazali, C. R. Murray, and T. Pohl, Polariton exchange interactions in multichannel optical networks, Phys. Rev. Lett. **123**, 113605 (2019); M. Khazali, K. Heshami, and C. Simon, Photon-photon gate via the interaction between two collective Rydberg excitations, Phys. Rev. A **91**, 030301(R) (2015); Single-photon source based on Rydberg exciton blockade, J. Phys. B **50**, 215301 (2017).

[27] M. Khazali, All-optical quantum information processing via a single-step Rydberg blockade gate, Opt. Express **31**, 13970 (2023).

[28] M. Khazali and W. Lechner, Scalable quantum processors empowered by the Fermi scattering of Rydberg electrons, Commun. Phys. **6**, 57 (2023).

[29] M. Khazali, Subnanometer confinement and bundling of atoms in a Rydberg empowered optical lattice, arXiv:2301.04450v1.

[30] M. Khazali, Photonic interface for long-distance entanglement of logical-qubits, arXiv:2204.08522v1.

[31] S. Puri *et al.*, Bias-preserving gates with stabilized cat qubits, Sci. Adv. **6**, eaay5901 (2020).